Tunneling vortex dynamics in linearly coupled Bose-Hubbard rings

Albert Escrivà,[1,2,*] Antonio Muñoz Mateo [1,3] Montserrat Guilleumas,[1,2] and Bruno Juliá-Díaz [1,2]

[1]*Departament de Física Quàntica i Astrofísica, Facultat de Física, Universitat de Barcelona, Martí i Franquès 1, 08028 Barcelona, Spain*
[2]*Institut de Ciències del Cosmos, Universitat de Barcelona, Martí i Franquès 1, 08028 Barcelona, Spain*
[3]*Graduate School, China Academy of Engineering Physics, 100193 Beijing, China*

The quantum dynamics of population-balanced fractional vortices and population-imbalanced vortices in an effective two-state bosonic system, made of two coupled discrete circuits with few sites, is addressed within the Bose-Hubbard model. We show that, for low on-site interaction, the tunneling of quantized vortices between the rings performs a coherent, oscillating dynamics connecting current states with chiral symmetry. The vortex-flux transfer dually follows the usual sinusoidal particle current of the Josephson effect, in good agreement with a mean-field approximation. Within such a regime, the switch of persistent currents in the rings resembles flux-qubit features and is feasible for experimental realization. On the contrary, strong interatomic interactions suppress the chiral current and lead the system into fragmented condensation.

I. INTRODUCTION

The recent advances in the preparation and control of ultracold atomic gases have fostered the appearance of a specific subfield termed atomtronics, which is aimed at the development of technological applications based on atomic matter waves [1–3]. Its first steps are mainly pursuing successfully applied theories from the fields of quantum optics and electronics, but also exploiting the ability of degenerate quantum gases to simulate other complex quantum systems [4].

In the search for basic tools that could eventually realize functional atomtronic devices, superconducting technologies are especially inspiring. This is due to the fact that the underlying condensates of superconducting electron pairs find their counterpart in the electrically neutral, ultracold Bose-Einstein condensates (BECs) of bosonic atoms, or even of paired fermionic atoms in the BCS-BEC crossover. Since the first experimental realizations of ring-trapped BECs, atomic circuits have been built to support persistent currents [5–8] and also to mimic the performance of the versatile superconducting quantum interference devices in atomtronic devices [9,10]. In particular, the feasibility of trapping ultracold atoms in looped geometries allows us to use the bosonic systems to explore the emulation of the superconducting flux qubits used in quantum computing [11]. Flux qubits are based on the switch of persistent currents flowing through Josephson junctions in a looped circuit threaded by magnetic flux. The role of the magnetic fluxoid in superconducting devices can be played by rotation-induced vortices in neutral bosonic systems. The entry or the exit of a vortex in the loop induces a change in the quantized circulating current that drives the system into a different metastable state. This scenario can lead to a candidate flux qubit if the two states connected by

the vortex transit are sufficiently isolated and if a coherent quantum dynamics of the system, oscillating between the two states, is achievable.

The search for plausible realizations of bosonic flux qubits has attracted great attention in the ultracold atomic gas community. Several proposals have explored looped one-dimensional geometries in both discrete [12–15] and continuous systems [16,17]. Within a mean-field framework, Refs. [12,18] have elaborated on plausible implementations of bosonic qubits. In spinor condensates, Refs. [19–21] showed the coherent transfer of half vortices between the condensate components, Refs. [22,23] analyzed Josephson oscillations in the angular momentum, and in Ref. [24] the dynamics of quantized currents has also been studied within the Bogoliubov approximation. On the other hand, there are many works based on a Bose-Hubbard (BH) ladder, where vortices can be generated by means of artificial magnetic fields [25–29]. The system dynamics can evolve into the one-dimensional equivalent of a superconducting vortex lattice [30] with an associated Meissner-vortex phase transition [31]. Recently, this ultracold-gas Meissner effect has been realized in laboratory experiments [32].

The present work contributes to the search of coherent quantum dynamics of vortices in bosonic circuits. Our setting makes use of two linearly coupled, discrete rings with a low number of sites, whose static properties have been previously reported in Ref. [33]. By means of a BH model, we explore the quantum dynamics of population-imbalanced vortices and population-balanced fractional vortices in double rings with different intra- to inter-ring coupling ratios and on-site interaction strengths. Different from regular, stationary vortex states, we search for realistic parameters in nonequilibrium, interacting systems of this type that allow for a regime of coherent oscillations of the initial vortex phase between the two rings. We explore different dynamical regimes and we show that there exists a range of parameters for low interactions where the transfer of vortex states between the two rings is coherent.

*albert.escriva@fqa.ub.edu

The paper is organized as follows. In Sec. II we describe the Hamiltonian of the system and present its characteristic parameters; we also introduce the analytical vortex solutions of the single-particle problem that is used to build many-particle imbalanced vortices and fractional vortices. In Sec. III we address the many-body problem of such nonstationary vortex solutions and identify their different dynamical regimes. Finally, Sec. IV gathers our conclusions and prospections for future work.

II. THEORETICAL MODEL

We consider N bosons loaded in two parallel Bose-Hubbard rings with M sites per ring. The coupling between rings, $J_\perp$, connects only sites with equal azimuthal coordinates. Inside each ring, there is a coupling J between next-neighbor sites. As a result, the system is described by the following Hamiltonian,

$$\hat{\mathcal{H}} = \sum_{l=0}^{M-1} \left[-J \sum_{j=\uparrow,\downarrow} (\hat{a}_{l,j}^\dagger \hat{a}_{l+1,j} + \hat{a}_{l+1,j}^\dagger \hat{a}_{l,j}) \right.$$
$$\left. -J_\perp (\hat{a}_{l,\uparrow}^\dagger \hat{a}_{l,\downarrow} + \hat{a}_{l,\downarrow}^\dagger \hat{a}_{l,\uparrow}) + \frac{U}{2} \sum_{j=\uparrow,\downarrow} \hat{n}_{l,j}(\hat{n}_{l,j}-1) \right], \quad (1)$$

where the bosonic creation and annihilation operators for the site l in the ring j (with $j =\uparrow,\downarrow$) are $\hat{a}_{l,j}^\dagger$ and $\hat{a}_{l,j}$, respectively. They fulfill the canonical commutation relations $[\hat{a}_{l,j}, \hat{a}_{m,k}^\dagger] = \delta_{lm}\delta_{jk}$. The corresponding number operators are $\hat{n}_{l,j} = \hat{a}_{l,j}^\dagger \hat{a}_{l,j}$, and the on-site atom-atom contact interaction strength is assumed to be repulsive, $U > 0$.

From the Hamiltonian (1), we construct the time evolution operator, $\hat{U}(t) = \exp(-i\hat{\mathcal{H}}t/\hbar)$, that propagates in real time an initial many-body state with N bosons, $|\Psi(t=0)\rangle$, as $|\Psi(t)\rangle = \hat{U}(t)|\Psi(t=0)\rangle$. We compute this action by means of the SCIPY implementation of the algorithm developed in Ref. [34]. At fixed time during the dynamical evolution, we measure the population imbalance between rings $z(t)$, the transition amplitude to a particular state $P(t)$, and the chiral current $\hat{L}_{\text{chi}}(t)$, which informs us on the angular momentum (vorticity) imbalance between rings.

The population imbalance $z(t) \in [-1, 1]$ is calculated as

$$z(t) = \frac{N_\uparrow(t) - N_\downarrow(t)}{N}, \quad (2)$$

where $N_j(t) = \sum_{l=0}^{M-1} \langle \Psi(t)|\hat{n}_{l,j}|\Psi(t)\rangle$ is the average number of atoms in the j ring. The total number of atoms in the system is a conserved quantity, $N = N_\uparrow(t) + N_\downarrow(t)$.

The probability of finding a particular target state, $|\Psi_{\text{target}}\rangle$, reads

$$P(t) = |\langle \Psi_{\text{target}}|\Psi(t)\rangle|^2. \quad (3)$$

The total azimuthal current is given by $\hat{L} = \hat{L}_\uparrow + \hat{L}_\downarrow$, where the azimuthal current in ring j is given by

$$\hat{L}_j = -i\frac{J}{\hbar} \sum_{l=0}^{M-1} (\hat{a}_{l,j}^\dagger \hat{a}_{l+1,j} - \hat{a}_{l+1,j}^\dagger \hat{a}_{l,j}). \quad (4)$$

From these operators, we define the chiral current operator as the difference in azimuthal current (or relative azimuthal current) between the two rings, $\hat{L}_{\text{chi}} = \hat{L}_\uparrow - \hat{L}_\downarrow$, and compute the mean chiral current, normalized to its initial value, as the nondimensional quantity

$$L_{\text{chi}}(t) = \frac{\langle \Psi(t)|\hat{L}_{\text{chi}}|\Psi(t)\rangle}{|\langle \Psi(0)|\hat{L}_{\text{chi}}|\Psi(0)\rangle|}. \quad (5)$$

The condensed fraction and the fragmentation of an N-particle many-body state is characterized by the normalized eigenvalues $p_l = N_l/N$, where N_l are the eigenvalues of the one-body density matrix $\hat{\rho}$ [35]. The matrix elements of the latter are given by

$$\rho_{(l,j),(m,k)} = \langle \Psi|\hat{a}_{l,j}^\dagger \hat{a}_{m,k}|\Psi\rangle, \quad (6)$$

so that $\sum_{l=1}^{2M} p_l = 1$. We henceforth refer to fragmentation when there are more than one eigenstates of order one, $p_l \propto O(1)$, even though the small number of particles in the systems considered does not properly allows us to state that there exists a macroscopic occupation of eigenstates.

A. Single-particle vortices and fractional vortices

The single-particle dispersion (at $U = 0$) of the Hamiltonian (1) contains two energy branches, $\epsilon_q^\pm = -2J\cos(2\pi q/M) \mp J_\perp$, that correspond to Bloch waves [25,33,36]

$$|\Psi_q^\pm\rangle = \frac{1}{\sqrt{2M}} \sum_{l=0}^{M-1} e^{i\frac{2\pi q l}{M}} (\hat{a}_{l,\uparrow}^\dagger \pm \hat{a}_{l,\downarrow}^\dagger)|\text{vac}\rangle, \quad (7)$$

where the integer quasimomentum takes the values $q = 0, \pm 1, \pm 2, \ldots, \lfloor M/2 \rfloor$, e.g., $q = 0, \pm 1$ for $M = 3$, and $q = 0, \pm 1, 2$ for $M = 4$.

Both energy branches $\epsilon_q^\pm$ belong to eigenstates of the total current operator with eigenvalues $L_q = 2J\sin(2\pi q/M)/\hbar$ and present zero chiral current. For a large number of sites M, the mentioned eigenvalues tend to $L_q/(4\pi J/M\hbar) = q$. We refer to these states as stationary (or regular) vortices of charge q. The vortices $|\Psi_q^-\rangle$ in the higher-energy branch ϵ_q^- present π-phase-shifted rings.

When the inter-ring coupling tends to zero, $J_\perp \to 0$, the eigenfunctions $|\Psi_q^\pm\rangle$ tend to be energetically degenerate, and the linear combinations $(|\Psi_q^+\rangle \pm |\Psi_q^-\rangle)/\sqrt{2}$ approximate stationary states with currents localized in one of the rings j, explicitly,

$$|\Psi_{q,j}\rangle = \hat{\Psi}_{q,j}^\dagger|\text{vac}\rangle \equiv \frac{1}{\sqrt{M}} \sum_{l=0}^{M-1} e^{i\frac{2\pi q l}{M}} \hat{a}_{l,j}^\dagger|\text{vac}\rangle, \quad (8)$$

whereas the other ring is empty. These states are only stationary in the (noninteracting) limit of decoupled rings and are referred as vortices of charge q with full imbalance $z = 1$ ($z = -1$), when $j =\uparrow (\downarrow)$.

We also consider states that combine two different single vortices of the type in Eq. (8), with charges q and q', which are loaded one in each ring to give a balanced $z = 0$

system as

$$|\Psi_{(q,q')}\rangle = |\Psi_{q,\uparrow}\rangle \otimes |\Psi_{q',\downarrow}\rangle$$

$$= \left(\sum_{l=0}^{M-1} \frac{e^{i\frac{2\pi q l}{M}}}{\sqrt{M}} \hat{a}_{l,\uparrow}^{\dagger}\right) \otimes \left(\sum_{l=0}^{M-1} \frac{e^{i\frac{2\pi q' l}{M}}}{\sqrt{M}} \hat{a}_{l,\downarrow}^{\dagger}\right) |\text{vac}\rangle. \quad (9)$$

Again, the resulting states are stationary only in the limit of (noninteracting) decoupled rings. The particular case with $q = 1$ and $q' = 0$ is the minimal example, carrying half the current of a regular vortex, $L_q/2$, and corresponds to the so-called half quantum vortex of a continuous system (see, e.g., Refs. [20,21] and [37] for the properties of these vortex states and their relation with domain walls of the relative phase in two-component condensates). For general (q, q'), due to the fractional value of the associated total azimuthal current, we will refer to states (9) as population-balanced, fractional-vortex states. Note that these states, as well as the imbalanced vortices discussed before, carry in the general case both nonzero total azimuthal current [as regular vortices of Eq. (7)] and nonzero chiral current (different from regular vortices).

B. Mean-field ansatz for the large-particle-number limit

The effect of the population imbalance on the many-body dynamics, as present in the imbalanced vortex states of Eq. (8), can be characterized within a mean-field approximation when the total number of particles N is large. In this case, the many-body state can be expressed as a coherent macroscopic superposition of equal states in the top, $|\Psi_{q,\uparrow}\rangle = \hat{\Psi}_{q,\uparrow}^{\dagger}|\text{vac}\rangle$, and in the bottom, $|\Psi_{q,\downarrow}\rangle = \hat{\Psi}_{q,\downarrow}^{\dagger}|\text{vac}\rangle$, rings [38]:

$$|\Psi(t)\rangle = \frac{1}{\sqrt{N!}}\left(\sqrt{\frac{1+z}{2}} e^{i\phi/2} \hat{\Psi}_{q,\uparrow}^{\dagger}\right.$$

$$\left. + \sqrt{\frac{1-z}{2}} e^{-i\phi/2} \hat{\Psi}_{q,\downarrow}^{\dagger}\right)^N |\text{vac}\rangle, \quad (10)$$

where $z(t)$ is the population imbalance and $\phi(t)$ is the average phase difference between the two rings. From this ansatz, the expectation value of the Hamiltonian (1) $\langle\mathcal{H}\rangle = \langle\Psi|\hat{\mathcal{H}}|\Psi\rangle/NJ_\perp$, in units of $NJ_\perp$, can be approximated by

$$\langle\mathcal{H}\rangle = \frac{\epsilon_q}{J_\perp} - \sqrt{1-z^2}\cos\phi + \frac{M\Lambda}{2}(1+z^2), \quad (11)$$

where $\epsilon_q = -2J\cos(2\pi q/M)$. The imbalance and the relative phase are canonically conjugate variables. From Eq. (11) the following equations of motion can be obtained:

$$\frac{dz}{d\tilde{t}} = -\sqrt{1-z^2}\sin\phi,$$

$$\frac{d\phi}{d\tilde{t}} = M\Lambda z + \frac{z}{\sqrt{1-z^2}}\cos\phi, \quad (12)$$

where we have defined the dimensionless time $\tilde{t}$, in units of the Rabi period, $t_R = \pi\hbar/J_\perp$, and the dimensionless interaction parameter Λ by

$$\tilde{t} = \frac{2\pi t}{t_R} = \frac{2J_\perp}{\hbar}t, \quad (13)$$

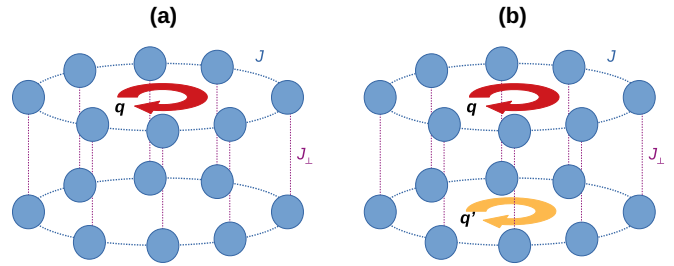$$\Lambda = \frac{(N-1)}{2M}\frac{U}{J_\perp}. \quad (14)$$

FIG. 1. Schematic picture of the two different initial states considered. Configuration A (left): Fully population-imbalanced ($z = 1$) vortex state of charge q in the top ring. Configuration B (right): Population-balanced fractional vortex of charges q and q' in the top and bottom rings, respectively.

Note that Eqs. (12) are the typical equations of a single, short bosonic Josephson junction [12], since the ansatz (10) involves only average quantities of the two rings. Despite the fact that the real dynamics of the system corresponds instead to a long Josephson junction [36] (where the tunneling between rings is site dependent), we show that this mean-field ansatz provides a good approximation when the interparticle interactions are low (against tunneling) and the evolution is constrained to a few periods of t_R. In any case, as we will see, the natural parameters t_R and Λ of this model are relevant parameters for identifying the dynamical regimes of the system.

III. IMBALANCED-VORTEX AND FRACTIONAL-VORTEX DYNAMICS

We investigate the coherent quantum tunneling between the two coupled rings of population-imbalanced vortices and population-balanced fractional vortices. We consider as initial configuration the two types of many-body states schematically depicted in Fig. 1. In configuration A (on the left in Fig. 1), we prepare a fully imbalanced, $z(0) = 1$, vortex state of charge q in the top ring, whereas the bottom ring is initially unpopulated. On the other hand, in configuration B (on the right in Fig. 1), we prepare a fully balanced state, $z(0) = 0$, that combines different vortices of charges q and q' in different rings. In both configurations, unless explicitly stated otherwise, we assume that the preparation of the initial state takes place at the zero inter-ring coupling $J_\perp = 0$ and the zero interaction strength $U = 0$. The subsequent time evolution of the system is monitored after switching on, instantaneously, particular nonzero values of $J_\perp$ and U. We search for the regime of coherent exchange of phase between the two coupled rings.

For completeness, we also present two cases that simulate a more realistic experimental procedure by using as initial states interacting stationary vortices, so that only a single parameter has to be instantaneously switched on. As we will see, maybe counterintuitively, these alternative initial conditions make a marginal difference with respect to the noninteracting ansatz in the observed dynamics, reflecting that the key feature for the few-particle systems considered is encoded in the translational invariance and phase profile of the initial vortex state.

For later comparison, it is useful to analyze first the tunneling dynamics of single-particle vortices. Let us assume an initial configuration of type A, without population in the bottom ring:

$$|\Psi^{(q)}(t=0)\rangle = |\Psi_{q,\uparrow}\rangle. \tag{15}$$

After switching on a nonzero coupling $J_\perp$, the time evolution of this state shows the coherent transfer of vorticity between the rings according to

$$|\Psi^{(q)}(t)\rangle = e^{-i\frac{\epsilon_q t}{\hbar}}[\cos(J_\perp t/\hbar)|\Psi_{q,\uparrow}\rangle$$
$$+ i\sin(J_\perp t/\hbar)|\Psi_{q,\downarrow}\rangle]. \tag{16}$$

The population imbalance evolves periodically in time as

$$z(t) = \cos(2J_\perp t/\hbar), \tag{17}$$

and the probability amplitude to find a fully imbalanced vortex in the bottom ring can be obtained from the target state $|\Psi_{\text{target}}\rangle = |\Psi_{q,\downarrow}\rangle$ as

$$P(t) = |\langle\Psi_{\text{target}}|\Psi^{(q)}(t)\rangle|^2 = \sin^2(J_\perp t/\hbar). \tag{18}$$

The non-normalized chiral current, which accounts for the phase (hence momentum) exchange between rings, reads

$$L_{\text{chi}}^{(q)}(t) = \frac{2J}{\hbar}\sin\left(\frac{2\pi q}{M}\right)\cos(2J_\perp t/\hbar) \tag{19}$$

and follows the population exchange (17). For a large number of sites, $2\pi q/M \ll 1$, the initial chiral current tends to $\langle\Psi_{q,\uparrow}|\hat{L}_{\text{chi}}|\Psi_{q,\uparrow}\rangle = (4\pi J/\hbar M)q$, which gives the relative azimuthal current between the two rings and is quantized in integer units of $(4\pi J/\hbar M)$.

As expected, this is the typical dynamical evolution of two linearly coupled quantum systems. The single-particle results are independent of the number of sites and (when normalized to initial state values) also of the intraring tunneling rate J and the vortex charge q. We will see that this coherent scenario cannot always be kept when interparticle interactions are taken into account.

It is also interesting to compare this single-particle estimate with the semiclassical prediction (12). For the vanishing interaction parameter $\Lambda \to 0$, the mean-field time evolution of the imbalance is harmonic, $\ddot{z} + \omega^2 z = 0$, with the angular frequency $\omega = 2\pi t_R^{-1}$, hence consistent with Eq. (17). The opposite limit of dominant interaction leads to anharmonic oscillations $\ddot{z} + z\sqrt{1-z^2}M\Lambda\cos\phi = 0$ that at high imbalance $z \to 1$ are suppressed ($\ddot{z} \approx \dot{z} \approx 0$) in a self-trapping regime.

For configuration B, the initial single-particle fractional vortices

$$|\Psi^{(q,q')}(t=0)\rangle = |\Psi_{q,\uparrow}\rangle \otimes |\Psi_{q',\downarrow}\rangle \tag{20}$$

evolve as

$$|\Psi^{(q,q')}(t)\rangle\!\rangle = e^{-i\frac{\epsilon_q t}{\hbar}}[\cos(J_\perp t/\hbar)|\Psi_{q,\uparrow}\rangle + i\sin(J_\perp t/\hbar)|\Psi_{q,\downarrow}\rangle]$$
$$\otimes\, e^{-i\frac{\epsilon_{q'} t}{\hbar}}[\cos(J_\perp t/\hbar)|\Psi_{q',\downarrow}\rangle$$
$$+ i\sin(J_\perp t/\hbar)|\Psi_{q',\uparrow}\rangle], \tag{21}$$

and the population balance, $z = 0$, persists during the whole time evolution. From the target state $|\Psi_{\text{target}}\rangle = \hat{\Psi}_{q',\uparrow}^\dagger \otimes$ $\hat{\Psi}_{q,\downarrow}^\dagger|\text{vac}\rangle$, the resulting transition probability, which monitors the transfer of the vortices, produces the same result (18) as configuration A. The same happens for the non-normalized chiral current

$$L_{\text{chi}}^{(q,q')}(t) = \frac{2J}{\hbar}\left[\sin\left(\frac{2\pi q}{M}\right) - \sin\left(\frac{2\pi q'}{M}\right)\right]\cos(2J_\perp t/\hbar), \tag{22}$$

when normalized to its initial value. Therefore, after normalization, the noninteracting phase-current dynamics turns out to be independent of the initial state choice of A or B, the latter one irrespective of the selected values q and q', as well. Again, for a large number of sites when $2\pi q/M \ll 1$ and $2\pi q'/M \ll 1$, Eq. (22) tends at $t=0$ to $[\langle\Psi_{q',\downarrow}| \otimes \langle\Psi_{q,\uparrow}|]\hat{L}_{\text{chi}}[|\Psi_{q,\uparrow}\rangle \otimes |\Psi_{q',\downarrow}\rangle] = (4\pi J/\hbar M)(q - q')$.

A. Many-body population-imbalanced vortex

We consider the initial many-body state to be a vortex of charge q in the top ring with imbalance $z(0) = 1$ (configuration A). That is, at $t=0$ all the atoms are populating the vortex state in the top ring and the bottom one is empty. In an N-particle bosonic system, in analogy with Eq. (8), the noninteracting $\Lambda = 0$, population-imbalanced vortex is given by

$$|\Psi_N^{(q)}\rangle = \frac{1}{\sqrt{N!}}(\hat{\Psi}_{q,\uparrow}^\dagger)^N|\text{vac}\rangle. \tag{23}$$

It is worth remarking that this is not an eigenstate of the total Hamiltonian Eq. (1), even in the noninteracting case, since its evolution,

$$|\Psi_N^{(q)}(t)\rangle_{\Lambda=0} = \frac{1}{\sqrt{N!}}\big(e^{-i\frac{\epsilon_q t}{\hbar}}[\cos(J_\perp t/\hbar)\hat{\Psi}_{q,\uparrow}^\dagger$$
$$+ i\sin(J_\perp t/\hbar)\hat{\Psi}_{q,\downarrow}^\dagger]\big)^N|\text{vac}\rangle, \tag{24}$$

replicates the single-particle coherent transfer of the vortex state between the two rings, with the transition probability to the many-body target state $|\Psi_{\text{target}}\rangle = (1/\sqrt{N!})(\hat{\Psi}_{q,\downarrow}^\dagger)^N|\text{vac}\rangle$ given by $P(t) = [\sin(J_\perp t/\hbar)]^{2N}$.

Figure 2 shows our numerical results for the time evolution of the many-body state, Eq. (23), with the vortex charge $q = 1$, in a double-ring system with $M = 3$ and $J_\perp = 1$, for two different interparticle-interaction values parametrized by $\Lambda = 0.2$ and $\Lambda = 50$. The population imbalance (thick solid lines), as well as the three largest eigenvalues of the one-body density matrix, p_1, p_2, and p_3 (symbols), is represented as a function of time. The left, middle and right panels correspond to different values of the intraring tunneling ratio, $J/J_\perp = 0$, 1, and 10, respectively. Inside each panel, thus for each interaction and coupling value, different numbers of particles, $N = 6$, 12, and 24 (top, middle, and bottom, respectively), have been considered. The mean-field limit value of the imbalance, obtained by solving the two coupled equations (12), is also shown (thin dashed lines) for comparison. The latter features a bosonic Josephson junction within two distinct dynamical regimes determined by the values of Λ [39]. For small interactions, $\Lambda = 0.2$ [all panels of Fig. 2(a)], the dynamical evolution corresponds to a Josephson regime, where the population is coherently transferred between rings with an
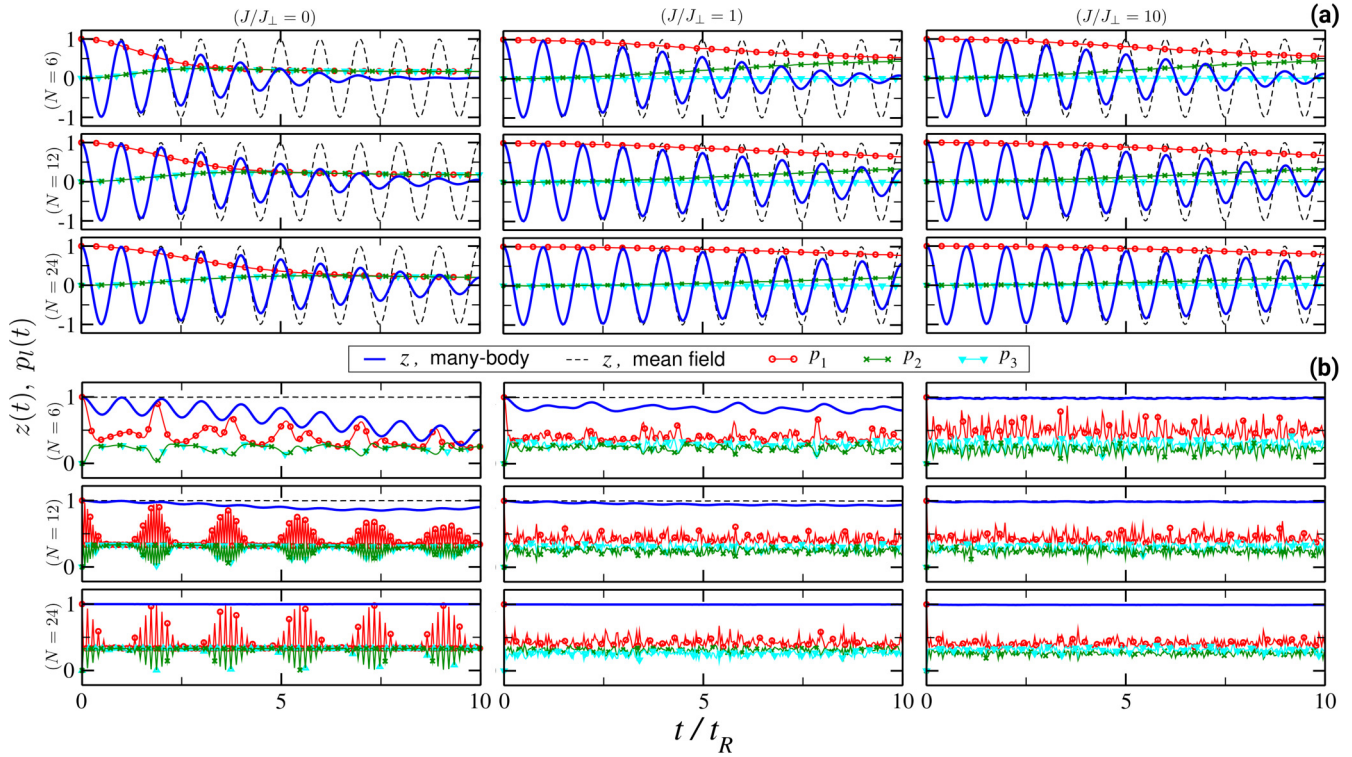
FIG. 2. Dynamical evolution of a fully imbalanced vortex of charge $q = 1$ for different values of $J/J_\perp$, N, and U. The top panels (a) correspond to $\Lambda = 0.2$, whereas the bottom panels (b) correspond to $\Lambda = 50$. In all cases, the number of sites of each ring is $M = 3$. The numerical solution for the population imbalance of the many-body quantum system (thick blue lines) is compared with the mean-field approximation given by Eqs. (12) (thin black dashed lines). The three largest eigenvalues of the one-body density matrix, p_1 (red circles), p_2 (green crosses), and p_3 (cyan triangles), are also plotted to monitor the condensed fraction and fragmentation of the system. The left, middle, and right panel groups correspond to intraring couplings $J/J_\perp = 0$, 1, and 10, respectively, for inter-ring coupling fixed to $J_\perp = 1$ in all panels. Time is measured in $t_R = \pi \hbar / J_\perp$ units.

oscillating imbalance around zero. On the contrary, for $\Lambda = 50$ [all panels of Fig. 2(b)], the system enters the self-trapping regime, where the particles remain mostly localized in one of the two rings. As can be seen, the many-body dynamics approaches more to the meanfield solution for an increasing number of particles [40].

By construction, the initial state (23) is fully condensed ($p_1 = 1$, $p_2 = p_3 = 0$). However, after switching on the interaction, the system loses its coherence and becomes fragmented during the time evolution, which is manifested by the loss of the imbalance amplitude with respect to the sinusoidal mean-field value and $p_1 < 1$. The opposite situation is achieved within the Josephson regime in the limit case of $J/J_\perp = 0$ (left panels in Fig. 2(a)], where the system tends at long times to a fully fragmented situation ($p_l = 1/6$, $\forall l$). The absence of intraring coupling $J = 0$ leads to trifragmentation inside each ring at a first stage, after which the imbalance gets damped.

Within the Josephson regime, the presence of intraring coupling $J/J_\perp > 0$ [middle and right panels in Fig. 2(a)] stretches the duration of the coherence ($p_1 \simeq 1$) exchange of phase and population between the rings. The resulting scenario does not change qualitatively with the particular value of nonzero J, and the long-time tendency shows that the lost of coherence leads to a bifragmented state ($p_1 = p_2 \simeq 1/2$ and $p_3 = 0$) reflecting the dynamics of two independent rings. For

longer times, not shown in the figure, revivals of the coherent oscillations are observed [41–43]. We have checked that such revivals appear before for higher-interaction values.

The large interaction $\Lambda = 50$ case, depicted in Fig. 2(b), is generally well characterized by the mean-field prediction of population self-trapping, and only a slight departure from this behavior is observed for $J = 0$ and $N = 6$, with the lowest number of particles. As a consequence, the coherence dynamical regimes shown in the low-interaction case are not reached at high interaction.

Additional details of the effects of the interatomic interaction on the system dynamics are provided in Fig. 3. The numerical time evolution of the chiral current, the population imbalance, the transition probability, and the density-matrix eigenvalues, is represented for a system with $N = 6$ atoms in the initial configuration A, with $q = 1$ and $J/J_\perp = 1$. Interaction values $U/J_\perp = 0.1$ (thick blue lines) and 100 (symbols) have been chosen to represent the Josephson and self-trapping regimes, and $U = 0$ (thin red lines) is also depicted for comparison. Although in the presence of interaction, fragmentation cannot be avoided during the time evolution, the coherent transfer of vorticity is still possible for short times at low interaction, when the intertunneling coupling dominates the dynamics. The transition probability provides a good signature of the lack of coherence at long times even for low interaction. As can be seen in the figure,
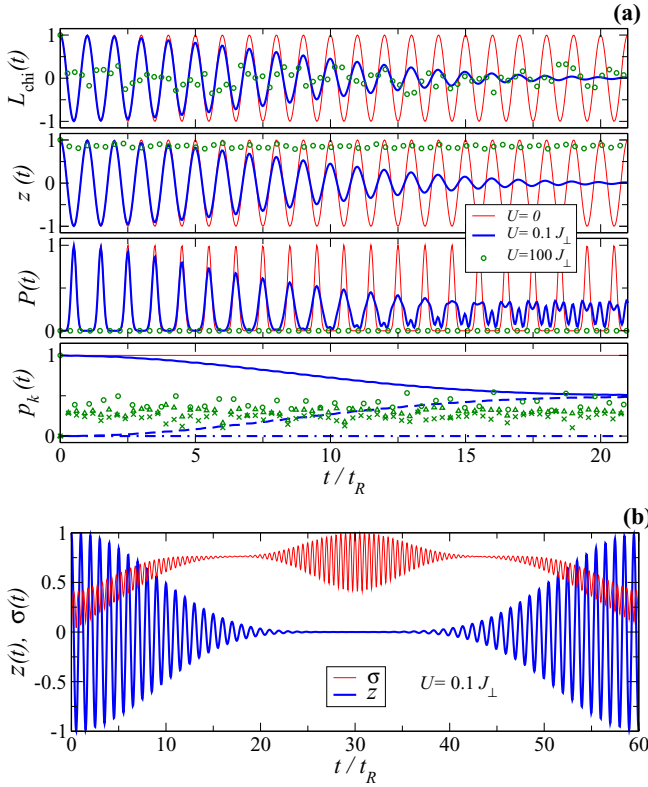
(a)

(b)

FIG. 3. (a) Dynamical observables during the time evolution of a fully imbalanced vortex state with $q = 1$, $N = 6$, $M = 3$, and $J/J_\perp = 1$, for several values of the ratio $U/J_\perp$: 0 (thin red line), 0.1 (thick blue lines), and 100 (symbols). From top to bottom: Normalized chiral current, population imbalance, transition probability, and the three largest eigenvalues of the one-body density matrix (p_1, p_2, p_3). (b) Long time evolution of the population imbalance, mean value (thick blue curve) and fluctuation (thin red curve), for the same setting and $U/J_\perp = 0.1$, showing the revival of the initial quantum state. Different from panel (a), the initial state is an interacting stationary vortex in a single ring. Time is measured in $t_R = \pi \hbar / J_\perp$ units.

the characteristic sinusoidal character of the vortex transfer is lost around $t \simeq 10 \, t_R$, when there is not a single dominant eigenvalue of the density matrix.

To obtain a more complete picture of the quantum dynamics, Fig. 3(b) exhibits the average and fluctuation values of the population imbalance for $U/J_\perp = 0.1$, during a long time evolution that includes the revival of the initial quantum state. Contrasting with Fig. 3(a), and for the sake of simulating more realistic experimental conditions, an interacting stationary vortex state in a single ring has been prepared as the initial state. Although the outcome is almost indistinguishable from the evolution shown in Fig. 3(a), in this way only one parameter, the inter-ring coupling $J_\perp$, had to be suddenly turned on at the beginning of the time evolution. As can be seen, the uncertainty in the average imbalance $\sigma = \sqrt{\langle z^2 \rangle - \langle z \rangle^2}$ grows when the semiclassical approximation fails, at the end of the coherent oscillations. Afterwards, interestingly, there is a regime of maximum variation in the uncertainty associated with a zero average imbalance that precedes the revival of the initial quantum state, in agreement with the literature [41,43].
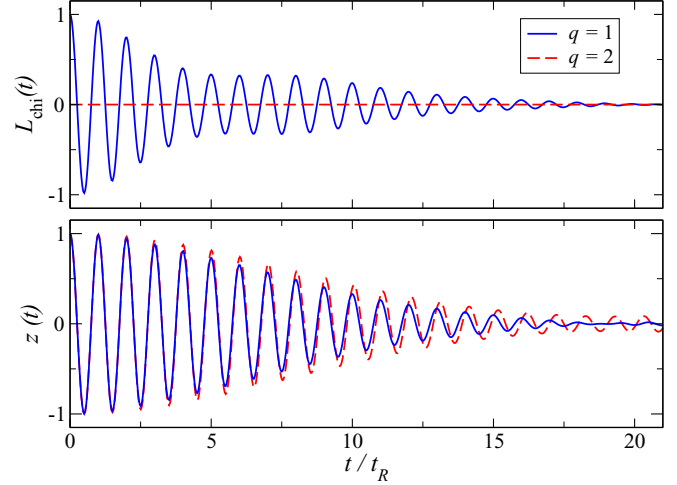

FIG. 4. Dynamical evolution of the normalized chiral current $L_{\rm chi}(t)$ and the population imbalance $z(t)$ of a fully imbalanced vortex state of charge $q = 1$ (blue solid line) and charge $q = 2$ (red dashed line) in a setting with $U/J_\perp = 0.1$, $J/J_\perp = 1$, $N = 6$, and $M = 4$.

During the whole evolution, the uncertainty oscillates twice as fast as the average imbalance, reaching minima when the absolute value of the average imbalance is maximum and reaching maxima when the average imbalance is zero.

We have also considered the dynamics of a population-imbalanced vortex (initial configuration A) in a noncommensurate system, having $M = 4$ sites per ring and $N = 6$ atoms, within the Josephson regime of $U/J_\perp = 0.1$ and $J/J_\perp = 1$. This system allows one to compare between different initial vortex charges: $q = \pm 1$ and $q = 2$ (see Fig. 4). Although the latter state does not carry any azimuthal current (since it lies at the edge of the Brillouin zone determined by the discrete lattice [44]) and also $L_{\rm chi}(t) = 0$, the time evolution of its population imbalance presents practically the same oscillatory behavior as the singly quantized vortices.

B. Many-body population-balanced fractional vortices

We consider now the initial configuration B: the same number of atoms $N/2$ per ring and different vortices of charges q and q' in the rings. The initial many-body state is described by

$$\left| \Psi_N^{(q,q')} \right\rangle = \frac{1}{(N/2)!} [(\hat{\Psi}_{q,\uparrow}^\dagger)^{\frac{N}{2}} \otimes (\hat{\Psi}_{q',\downarrow}^\dagger)^{\frac{N}{2}}] |{\rm vac}\rangle. \tag{25}$$

This initial state is bifragmented with $p_1(t = 0) = p_2(0) = 1/2$.

In Fig. 5 we show the numerical results for an initial half-vortex state with $(q, q') = (1, 0)$ and different values of the interaction $U/J = 0.1$ and 100. The noninteracting dynamics (red lines) is also shown for comparison. Contrary to configuration A, this case only presents phase imbalance and not population imbalance between the rings, which according to the Josephson equations should translate into a particle current. However, one can see from Fig. 5 that it does not break the initial balance of population: $z(t) \simeq 0$ during the time evolution. Since the angular momentum carried by the tunneling particles is different in the top-to-bottom-ring
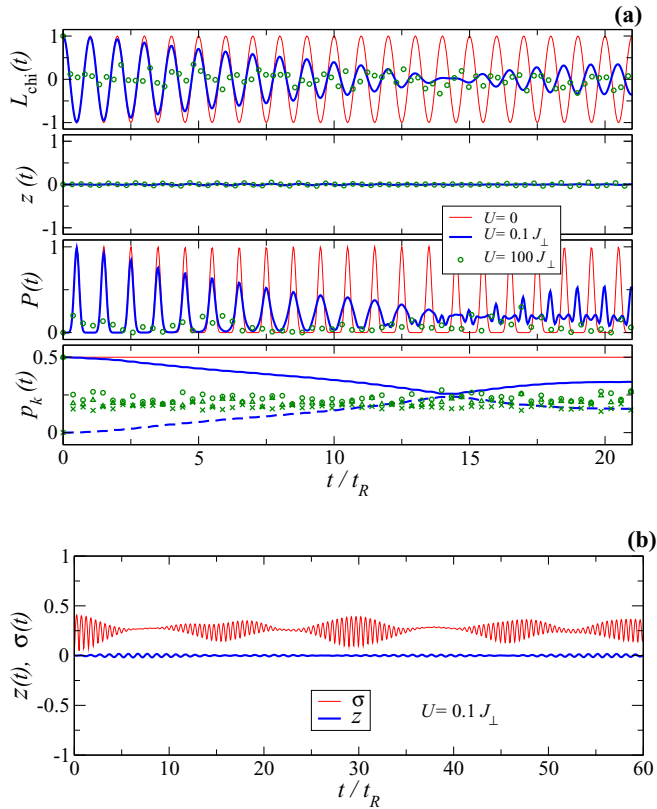
(a)

(b)

FIG. 5. Same as Fig. 3, in a setting with $M = 3$ and $N = 6$, for an initial state made of a population-balanced half vortex with charges $(q, q') = (1, 0)$. For $U = 0.1 J_\perp$ (respectively for $U = 0$), the eigenvalues of the one-body density matrix are almost (respectively exactly) doubly degenerate, showing overlapped curves during the time interval exhibited in the figure, that is, $p_1 \simeq p_2$ and $p_3 \simeq p_4$.

current from the bottom-to-top-ring current, a nonvanishing angular momentum difference, or chiral current, is transferred between the rings, as it is shown in the top panel of Fig. 5(a).

Despite the differences in the initial state, the outcome is qualitatively similar to the evolution already shown for configuration A, and the coherent phase transfer between rings (if present at early stages) is eventually suppressed due to the presence of interparticle interactions. For the small interactions $U/J_\perp = 0.1$ (thick blue lines in Fig. 5) the coherent behavior is preserved for a few Rabi cycles and also presents revivals (not shown in the figure) for longer times. Simultaneously, $L_{\text{chi}}(t)$ separates from the noninteracting result. Conversely, at large interaction values (symbols) the system becomes fragmented at the very beginning of the dynamics and tends to a six-fragmented state. In general, the direct comparison between Figs. 3 and 5 shows small differences in the chiral current or in the transition probability of configurations A and B. A distinctive feature, however, can be observed in the evolution of the population imbalance, whose uncertainty in configuration B, around essentially zero average imbalance [see Fig. 5(b)], presents a small variation even during the collapse of the coherent oscillations.

We have checked that an increase in the number of particles stretches the duration of the coherent-dynamics stage
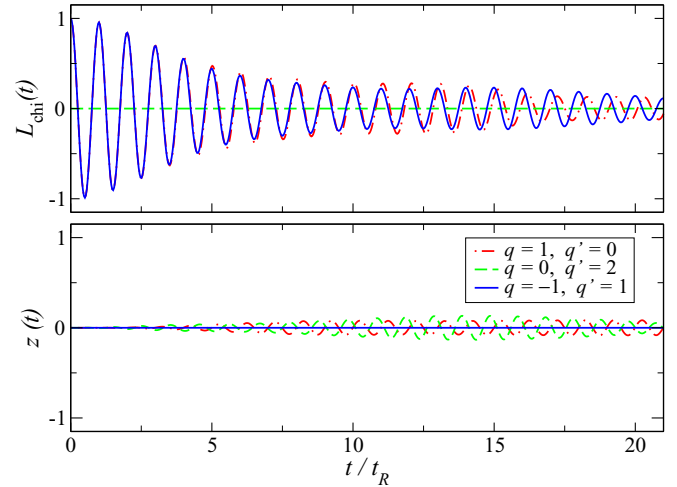

FIG. 6. Dynamical evolution of the chiral current $L_{\text{chi}}(t)$ and the population imbalance $z(t)$ for different fractional-vortex charges $(q, q') = (1, 0)$ (red dashed-dotted lines), $(0,2)$ (green dashed lines), and $(1, -1)$ (blue solid lines) and for the parameters $J/J_\perp = 1$, $N = 6$, $M = 4$, and $U/J_\perp = 0.1$.

in the Josephson regime. In this way, our results tend to previous results obtained within the mean-field framework [19], where long-duration coherent oscillations of half vortices were demonstrated in a two-component spinor condensate. Finally, we compare the fractional-vortex dynamics for several initial charges (q, q'). In Fig. 6 we show the chiral current and the population imbalance in a system with $M = 4$, $N = 6$, $J/J_\perp = 1$, and $U/J_\perp = 0.1$, as a function of time, for $(q, q') = (1, 0)$, $(0, 2)$, $(1, -1)$. As in the previous cases, the evolution of the dynamical properties is sinusoidal with period $t_R = \pi \hbar / J_\perp$. For $(1,0)$ and $(1, -1)$, the amplitude of the oscillations in the chiral current is smoothly damped, and only in the first Rabi cycles is there a quasicomplete exchange of the two initial vortex charges between the two rings. As expected for $(0,2)$, made of vortex states in a single ring situated at the center $q = 0$ and at the edge $q' = M/2$ of the Brillouin zone, there is no current and $L_{\text{chi}}(t) = 0$.

Figure 6 shows interesting differences in the population imbalance between $(1, -1)$, where it remains zero during the whole evolution, and the initial half-vortex states $(1,0)$ and $(0,2)$, where the population shows an oscillatory imbalance with varying amplitude. From general features of Josephson junctions, we attribute this different behavior to the differences in energy associated with the vortex charges involved in each configuration, since the Josephson equations predict that an energy variation across the junction modulates the particle current. Such modulation is absent in the $(1, -1)$ state, where the half vortices with charge 1 and -1 are energetically degenerate.

IV. CONCLUSIONS AND DISCUSSION

We have studied the quantum tunneling dynamics of many-body vortices in linearly coupled, discrete circuits. In a double-ring geometry, we have considered population-imbalanced vortices and population-balanced, fractional vortices that can first be obtained in a stationary configuration of

decoupled rings and later monitored through the observation of the population imbalance and the chiral particle flux during a coupled-ring dynamics.

The system preparation is well within the reach of current experimental techniques. Protocols for the generation of ring-ladder lattices and the readout of flux qubits have been given in the literature (see, e.g., Ref. [18]). The atoms could be loaded in two rings living in consecutive wells of a perpendicular, tilted optical lattice, whose depth controlled the on-off switch of inter-ring tunneling $J_\perp$, while the tilting provided the required initial population imbalance. By means of two-photon Raman processes, angular momentum could be imprinted on the atoms, and matter wave interferometry after time-of-flight expansion could be used to observe the system phase patterns [45]. Alternatively, by using laser-assisted tunneling in the ring lattice, a spatially dependent complex tunneling could be imprinted to induce controlled vortex currents [46,47].

Our results show that, after preparing the initial vortices at low-interaction values, the subsequent dynamics is determined by the coherent oscillations of the initial vortex phase between the two rings, in the practically independent way of the initial vortex configuration. The vortex-flux connects current states with chiral symmetry and dually follows the usual sinusoidal particle current of the Josephson effect. The duration of the coherent regime increases with the number of particles, which makes the system more feasible for experimental realization. The high-interaction regime, however, suppresses the superfluid tunneling dynamics through population self-trapping.

It is worth mentioning that the vortex tunneling is also sensitive to the number of couplings between rings. We have checked that when there is only one such coupling, like in the experiment of Ref. [48], tunneling processes are drastically reduced. Nevertheless, the study of the vortex tunneling dynamics as a function of the number of couplings between the two rings is beyond the scope of this work and will be addressed elsewhere.

ACKNOWLEDGMENTS

[1] L. Amico, G. Birkl, M. Boshier, and L.-C. Kwek, New J. Phys. **19**, 020201 (2017).

[2] M. K. Olsen and A. S. Bradley, Phys. Rev. A **91**, 043635 (2015).

[3] B. T. Seaman, M. Krämer, D. Z. Anderson, and M. J. Holland, Phys. Rev. A **75**, 023615 (2007).

[4] I. M. Georgescu, S. Ashhab, and F. Nori, Rev. Mod. Phys. **86**, 153 (2014).

[5] C. Ryu, M. F. Andersen, P. Cladé, V. Natarajan, K. Helmerson, and W. D. Phillips, Phys. Rev. Lett. **99**, 260401 (2007).

[6] A. Ramanathan, K. C. Wright, S. R. Muniz, M. Zelan, W. T. Hill, C. J. Lobb, K. Helmerson, W. D. Phillips, and G. K. Campbell, Phys. Rev. Lett. **106**, 130401 (2011).

[7] S. Moulder, S. Beattie, R. P. Smith, N. Tammuz, and Z. Hadzibabic, Phys. Rev. A **86**, 013629 (2012).

[8] S. Beattie, S. Moulder, R. J. Fletcher, and Z. Hadzibabic, Phys. Rev. Lett. **110**, 025301 (2013).

[9] S. Eckel, J. G. Lee, F. Jendrzejewski, N. Murray, C. W. Clark, C. J. Lobb, W. D. Phillips, M. Edwards, and G. K. Campbell, Nature (London) **506**, 200 (2014).

[10] C. Ryu, P. W. Blackburn, A. A. Blinova, and M. G. Boshier, Phys. Rev. Lett. **111**, 205301 (2013).

[11] I. Chiorescu, Y. Nakamura, C. J. P. M. Harmans, and J. E. Mooij, Science **299**, 1869 (2003).

[12] D. Aghamalyan, L. Amico, and L. C. Kwek, Phys. Rev. A **88**, 063627 (2013).

[13] D. Aghamalyan, M. Cominotti, M. Rizzi, D. Rossini, F. W. J. Hekking, A. Minguzzi, L. C. Kwek, and Amico, New. J. Phys. **17**, 045023 (2015).

[14] D. W. Hallwood and J. Brand, Phys. Rev. A **84**, 043620 (2011).

[15] A. Gallemí, M. Guilleumas, J. Martorell, R. Mayol, A. Polls, and B. Juliá-Díaz, New J. Phys. **17**, 073014 (2015).

[16] C. Schenke, A. Minguzzi, and F. W. J. Hekking, Phys. Rev. A **84**, 053636 (2011).

[17] P. L. Halkyard, M. P. A. Jones, and S. A. Gardiner, Phys. Rev. A **81**, 061602(R) (2010).

[18] L. Amico, D. Aghamalyan, F. Auksztol *et al.*, Sci. Rep. **4**, 4298 (2015).

[19] A. Gallemí, A. Muñoz Mateo, R. Mayol, and M. Guilleumas, New J. Phys. **18**, 015003 (2016).

[20] M. Tylutki, L. P. Pitaevskii, A. Recati, and S. Stringari, Phys. Rev. A **93**, 043623 (2016).

[21] L. Calderaro, A. L. Fetter, P. Massignan, and P. Wittek, Phys. Rev. A **95**, 023605 (2017).

[22] I. Lesanovsky and W. von Klitzing, Phys. Rev. Lett. **98**, 050401 (2007).

[23] J. Brand, T. J. Haigh, and U. Zülicke, Phys. Rev. A **80**, 011602(R) (2009).

[24] A. Richaud and V. Penna, Phys. Rev. A **96**, 013620 (2017).

[25] D. Hügel and B. Paredes, Phys. Rev. A **89**, 023619 (2014).

[26] A. Tokuno and A. Georges, New J. Phys. **16**, 073005 (2014).

[27] M. Piraud, F. Heidrich-Meisner, I. P. McCulloch, S. Greschner, T. Vekua, and U. Schollwöck, Phys. Rev. B **91**, 140406(R) (2015).

[28] S. Uchino, Phys. Rev. A **93**, 053629 (2016).

[29] N. Victorin, F. Hekking, and A. Minguzzi, Phys. Rev. A **98**, 053626 (2018).

[30] E. Orignac and T. Giamarchi, Phys. Rev. B **64**, 144515 (2001).

[31] T. Haug, L. Amico, R. Dumke, and L.-C. Kwek, Quantum Sci. Technol. **3**, 035006 (2018).

[32] M. Atala, M. Aidelsburger, M. Lohse, M. T. Barreiro, B. Paredes, and I. Bloch, Nat. Phys. **10**, 588 (2014).

[33] A. Escrivà, B. Juliá-Díaz, and M. Guilleumas, arXiv:1807.03838.

[34] A. H. Al-Mohy and N. J. Higham, SIAM J. Sci. Comput. **33**, 488 (2011).

[35] E. J. Mueller, T.-L. Ho, M. Ueda, and G. Baym, Phys. Rev. A **74**, 033612 (2006).

[36] J. A. G. Granados, A. M. Mateo, M. Guilleumas, and X. Viñas, New J. Phys. **21**, 043036 (2019).

[37] D. T. Son and M. A. Stephanov, Phys. Rev. A **65**, 063621 (2002).

[38] P. Buonsante, R. Burioni, E. Vescovi, and A. Vezzani, Phys. Rev. A **85**, 043625 (2012).

[39] S. Raghavan, A. Smerzi, S. Fantoni, and S. R. Shenoy, Phys. Rev. A **59**, 620 (1999).

[40] B. Juliá-Díaz, D. Dagnino, M. Lewenstein, J. Martorell, and A. Polls, Phys. Rev. A **81**, 023615 (2010).

[41] R. Robinett, Phys. Rep. **392**, 1 (2004).

[42] G. J. Milburn, J. Corney, E. M. Wright, and D. F. Walls, Phys. Rev. A **55**, 4318 (1997).

[43] M. Greiner, O. Mandel, T. W. Hänsch, and I. Bloch, Nature (London) **419**, 51 (2002).

[44] A. Munoz Mateo, V. Delgado, M. Guilleumas, R. Mayol, and J. Brand, Phys. Rev. A **99**, 023630 (2019).

[45] J. F. S. Brachmann, W. S. Bakr, J. Gillen, A. Peng, and M. Greiner, Opt. Express **19**, 12984 (2011).

[46] M. Aidelsburger, M. Atala, M. Lohse, J. T. Barreiro, B. Paredes, and I. Bloch, Phys. Rev. Lett. **111**, 185301 (2013).

[47] H. Miyake, G. A. Siviloglou, C. J. Kennedy, W. C. Burton, and W. Ketterle, Phys. Rev. Lett. **111**, 185302 (2013).

[48] M. R. Sturm, M. Schlosser, R. Walser, and G. Birkl, Phys. Rev. A **95**, 063625 (2017).